Received: 22 February 2022 | Accepted: 10 May 2022

DOI: 10.1111/bpa.13083

RESEARCH ARTICLE

Brain Pathology

DNA methylation profiling of central nervous system hemangioblastomas identifies two distinct subgroups

Niklas Woltering[1] | Anne Albers[1] | Michael Müther[2] | Walter Stummer[2] | Werner Paulus[1] | Martin Hasselblatt[1] | Markus Holling[2] | Christian Thomas[1]

[1]Institute of Neuropathology, University Hospital Münster, Münster, Germany

[2]Department of Neurosurgery, University Hospital Münster, Münster, Germany

Correspondence
Christian Thomas, Institute of Neuropathology, University Hospital Münster, Pottkamp 2, 48149 Münster, Germany.
Email: christian.thomas@ukmuenster.de

Funding information
Deutsche Forschungsgemeinschaft, Grant/Award Number: TH 2345/1-1; Verein von Hippel-Lindau betroffener Familien eV., Grant/Award Number: N/A

Abstract

Hemangioblastomas (HBs) of the central nervous system are highly vascular neoplasms that occur sporadically or as a manifestation of von Hippel–Lindau (VHL) disease. Despite their benign nature, HBs are clinically heterogeneous and can be associated with significant morbidity due to mass effects of peritumoral cysts or tumor progression. Underlying molecular factors involved in HB tumor biology remain elusive. We investigated genome-wide DNA methylation profiles and clinical and histopathological features in a series of 47 HBs from 42 patients, including 28 individuals with VHL disease. Thirty tumors occurred in the cerebellum, 8 in the brainstem and 8 HBs were of spinal location, while 1 HB was located in the cerebrum. Histologically, 12 HBs (26%) belonged to the cellular subtype and exclusively occurred in the cerebellum, whereas 35 HBs were reticular (74%). Unsupervised clustering and dimensionality reduction of DNA methylation profiles revealed two distinct subgroups. Methylation cluster 1 comprised 30 HBs of mainly cerebellar location (29/30, 97%), whereas methylation cluster 2 contained 17 HBs predominantly located in non-cerebellar compartments (16/17, 94%). The sum of chromosomal regions being affected by copy-number alterations was significantly higher in methylation cluster 1 compared to cluster 2 (mean 262 vs. 109 Mb, $p = 0.001$). Of note, loss of chromosome 6 occurred in 9/30 tumors (30%) of methylation cluster 1 and was not observed in cluster 2 tumors ($p = 0.01$). No relevant methylation differences between sporadic and VHL-related HBs or cystic and non-cystic HBs could be detected. Deconvolution of the bulk DNA methylation profiles revealed four methylation components that were associated with the two methylation clusters suggesting cluster-specific cell-type compositions. In conclusion, methylation profiling of HBs reveals 2 distinct subgroups that mainly associate with anatomical location, cytogenetic profiles and differences in cell type composition, potentially reflecting different cells of origin.

KEYWORDS
hemangioblastoma, methylation profiling, von Hippel–Lindau disease

1 | INTRODUCTION

Hemangioblastomas (HBs) of the central nervous system (CNS) are highly vascular tumors predominantly arising in the cerebellum and the spinal cord [1]. They may either occur sporadically or (in 25% of cases) as a manifestation of von Hippel–Lindau (VHL) disease [2]. Sporadic cases usually present with solitary lesions, whereas VHL patients tend to develop multiple HBs, which requires lifelong medical surveillance [1]. Histologically, HBs are

Markus Holling and Christian Thomas contributed equally to this study.

characterized by a rich capillary network and large vacuolated stromal cells representing the neoplastic cell population [3]. They can be categorized into two subtypes: (i) reticular HBs with abundant capillaries and scattered stromal cells and (ii) cellular HBs with large clusters of uniform tumor cells being associated with a higher frequency of tumor progression [4]. Despite their designation as benign grade 1 tumors according to the World Health Organization (WHO) classification of CNS tumors [5], HBs are associated with significant morbidity due to mass effects of the primary tumor or the occurrence of (often large) peri-tumoral cysts [6, 7]. Recurrence or tumor progression is observed in some cases [8] and rarely, leptomeningeal dissemination may occur [9].

Mutations in the *VHL* tumor suppressor gene located on chr3p25.3 are long known to play a role in both sporadic and VHL disease related tumors [10–13], but genetic factors explaining the clinical heterogeneity of HBs remain uncertain. Despite copy-number alterations in a fraction of cases [10, 14], the exome of HBs is remarkably simple and devoid of additional oncogenic driver mutations [12, 13]. Transcriptome and lipidomic analysis of cystic and solid HBs revealed dysregulated lipid metabolism-related genes in cyst-forming tumors [15], but the underlying molecular alterations remain elusive. Recently, molecular characterization of the *VHL* promoter uncovered epigenetic differences in sporadic and VHL-associated HBs [10], raising the possibility that changes in DNA methylation might help to identify relevant biological subgroups. Genome-wide DNA methylation arrays have emerged as a powerful tool for robust classification of CNS tumors and for unsupervised identification of novel and potentially clinically relevant molecular subgroups [16, 17].

Therefore, we aimed to characterize methylation profiles and clinical and histopathological features in a larger series of sporadic and VHL-related HBs. Here, we show that methylation profiling of HBs reveals two molecular subgroups with distinct methylation components and differences in cytogenetic profiles.

2 | MATERIALS AND METHODS

2.1 | Materials

Formalin-fixed paraffin-embedded tumor samples of 47 HBs from 42 patients resected at the University Hospital Münster between 2009 and 2020 were retrieved from the archive of the Institute of Neuropathology Münster. Histopathology was reviewed according to 2021 WHO criteria. Tumors predominantly composed of zellballen-like cellular clusters of tumor cells with large epithelioid cells with finely granular cytoplasm were classified as "cellular" and tumors in which capillary networks prevailed were classified as "reticular" [4]. Clinical data were retrospectively determined and de-identified. Detailed follow-up data on recurrence (i.e. new or progressive lesions at the same anatomical compartment) was available for all 42 patients. Recurrence data were evaluated by Kaplan–Meier analysis and Log-Rank test. The use of biopsy-specimens for research upon anonymization was in accordance with local regulations of the University Hospital Münster and approved by the Münster ethics committee (2007-420-f-S and 2017-707-f-S).

2.2 | DNA methylation profiling

DNA was isolated after macrodissection of tumor tissue from formalin-fixed paraffin-embedded tumor samples. Following purification and bisulfite conversion using standard protocols provided by the manufacturer, samples were analyzed using the MethylationEPIC BeadChip array (Illumina Inc., San Diego, CA) as previously described [18]. Raw IDAT files were loaded into the R environment (v4.1.0) using the minfi package (v1.38.0). For genotype analyses, the getSnpBeta function was used to retrieve intensity values of 59 SNP probes. Pairwise sample-to-sample Pearson correlations were plotted with the pheatmap package (v1.0.12) and manual inspection showed high correlation of samples from the same individual (Figure S1). The following filtering criteria were applied: removal of probes targeting the X and Y chromosomes, removal of probes containing a single nucleotide polymorphism (MAF >1%) within five base pairs of and including the targeted CpG-site, and probes not uniquely mapping the human reference genome (hg19). In total, 749,312 CpG sites were kept for downstream analyses. DNA methylation-based classification was performed with the Heidelberg Brain Tumor Classifier (v11b4) [16]. DNA methylation data have been deposited in GEO (accession number GSE197378).

2.3 | Copy-number variation analysis

Copy-number variation (CNV) analysis from DNA methylation array data was facilitated using the conumee Bioconductor package after additional baseline correction (https://github.com/dstichel/conumee). Chromosome-wide gains and losses were visually assessed from CNV plots. Focal *VHL* deletions were defined as distinct copy number losses involving chr3:10,183,319-10,195,354 (hg19) with a notably higher amplitude than adjacent regions.

2.4 | Dimensionality reduction

Unsupervised *t*-distributed stochastic neighbor embedding (t-SNE) analysis was performed together with previously published [16] DNA methylation profiles of 2801 samples comprising 82 brain tumor entities (GEO

accession number GSE90496) using the Rtsne package (v0.15). The first 94 principal components (PCs) were calculated with singular value decomposition (SVD) and then used to perform the *t*-SNE analysis with the following parameter adjustments: pca = FALSE, max_iter = 2000, theta = 0. Uniform Manifold Approximation and Projection (UMAP) analysis of the HB cohort was performed using the umap package with default parameters (v0.2.7).

2.5 | Consensus clustering

Consensus clustering was performed on the matrix of beta values using the R/bioconductor package cola (version 1.99.4) [19]. Various combinations of feature selection and partitioning methods were adopted to fit consensus clustering models with k subgroups ranging from 2 to 6. Standard deviation (SD), coefficient of variance (CV), median absolute deviation (MAD) and ability to correlate to other rows (ATC) were used as feature selection methods. The following partitioning methods were used to separate samples into subgroups ranging from 2 to 6 classes: hierarchical clustering with cutree (hclust), k-means clustering (kmeans), spherical k-means clustering (skmeans), partitioning around medoids (pam) and model-based clustering (mclust). The models were assessed to determine the optimal fit using the mean silhouette score, the 1 - proportion of ambiguous clustering (PAC) score, concordance, and the Jaccard index. In addition, consensus heatmaps and membership heatmaps (illustrating the membership of every individual partition generated from random subsets of the original matrix) were visually inspected.

2.6 | VHL promoter methylation

As evidence of epigenetic silencing, the VHL promoter was considered methylated if the beta value for probe cg15267345 within the CpG Island exceeded 0.2 as previously published [20].

2.7 | Differential methylation

Differentially methylated CpG sites (DMCs) were calculated as previously described [21]. Given that small standard deviations at individual CpG sites frequently arise by chance and might result in highly significant, but often spurious results, an indiscriminate standard deviation cutoff of 0.05 was implemented to eliminate CpG sites with small standard deviations. The remaining 425,531 CpG sites were used for downstream statistical analysis. A nonparametric Mann–Whitney *U* test was used to identify CpGs that were differentially methylated between comparison groups. The *p*-values for the differentially methylated CpG sites were corrected for multiple hypothesis testing by the Benjamini-Hochberg procedure, and $q = 0.01$ was used as a threshold for significance. GO and KEGG enrichment analyses were performed using the gometh package (v1.1).

2.8 | Deconvolution analysis

Dissection of bulk DNA methylation profiles was performed with MeDeCom, a reference-free deconvolution algorithm that identifies major components of variation, termed latent methylation components (LMC) [22]. Methylation array data were processed according to a recently published protocol [23] using the 5000, 10,000, and 15,000 most variably methylated CpG sites across the samples as input to MeDeCom. Investigation of the cross-validation error and of the objective value for the parameter number of LMCs (kappa) and the regularization parameter (λ) were performed, resulting in a set of LMCs. Overall, the cross-validation error pointed to selecting 4 components (parameter *k*) and the regularization parameter λ as 0. Manual inspection of LMC distributions revealed tumor HB_42, the sample with the lowest methylation classifier score (calibrated score 0.3, Table S1), as a clear outlier and has thus been excluded from deconvolution analyses. Hierarchical clustering analysis of LMC proportions derived from each sample was performed using Euclidean distance and Ward's linkage. In addition, deconvolution analysis has been performed together with DNA methylation profiles of other VHL-related tumor entities including 12 endolymphatic sac tumors (ELST) (GSE168808) and 324 clear cell renal carcinomas (ccRCC) of the TCGA cohort (TCGA-KIRC). For a detailed deconvolution of the cellular composition of bulk HB samples, we applied the reference-based MethylCIBERSORT algorithm [24] to infer distinct cellular contents (endothelial cells, fibroblasts, CD14-positive cells, CD4- and CD8-positive T cells, regulatory T cells and neutrophils). The analysis was carried out on the Noob normalized beta matrix using the MethylCIBERSORT R package (v0.20) with a previously published reference matrix [25]. The beta matrix of HB samples and reference files were uploaded onto the CIBERSORT portal and deconvoluted (https://cibersort.stanford.edu/). Tumor purity of each sample was estimated using the RF_Purify algorithm [26].

3 | RESULTS

3.1 | Patient characteristics

The series comprised 47 HBs from 16 male and 26 female patients (Table 1). Twenty-eight HBs (60%) occurred in patients with VHL, four of which had multiple resections of individual HBs (Table S1). The median age at diagnosis of VHL patients was significantly younger compared

TABLE 1 Patient characteristics

	All cases (47 HBs of 42 patients)	Methylation cluster 1(30 HBs of 28 patients)	Methylation cluster 2 (17 HBs of 17 patients)	Significance
Sex (male/female)	16/26	10/20	8/9	n.s.*
Age (years) (median, range)	49 (15–84)	50 (24–84)	43 (15–78)	n.s.**
VHL disease related (%)	28 (60%)	17 (57%)	11 (65%)	n.s.**
Histology				
Cellular	12	12	0	$p = 0.003$*
Reticular	35	18	17	
Location				
Cerebellum	30	29	1	$p < 0.001$*
Brainstem	8	1	7	
Spinal	8	0	8	
Cerebral	1	0	1	
Peritumoral cyst (%)	34 (72%)	22 (73%)	12 (71%)	n.s.*
VHL promoter methylation	2	1	1	n.s.*
CNVs				
Mean CNV load (Mb)	206	262	109	$p = 0.001$**
Chr3p loss	26	18	8	n.s.*
Focal Chr3p25.3 deletion	18	10	8	
Balanced Chr3p	3	2	1	
Chr6 loss	9	9	0	$p = 0.01$*

Abbreviations: HB, Hemangioblastoma; CNV, copy-number variation; VHL, von Hippel-Lindau.
*Chi-square test.
**Student's *t*-test.

to patients with sporadic HBs (40 vs. 57 years, $p < 0.001$, Student's *t*-test). The majority of HBs were located in the cerebellum (30/47, 64%), whereas 8 tumors (17%) arose in the brain stem and 8 HBs (17%) occurred in the spinal cord. One sporadic HB was located in the cerebrum. There was no significant difference in tumor location comparing VHL patients to sporadic HB patients (n.s., chi-square test). Histologically, 12 HBs (26%) belonged to the cellular subtype and 35 were reticular (74%). Of note, the cellular HBs exclusively occurred in the cerebellum whereas all non-cerebellar HBs were reticular ($p = 0.003$, chi-square test). Histological subtype was not associated with VHL germline status (sporadic HBs: 6 cellular and 13 reticular; VHL-associated HBs: 6 cellular and 22 reticular; n.s., chi-square test).

3.2 | Copy-number variations

The most frequent recurrent copy-number alteration were losses of whole chromosome 3 or chromosome 3p (55%) and a focused analysis of the *VHL* locus on chr3p25.3 revealed focal deletions in 18 additional cases (38%) (Table S1, Figure S3). Other common CNVs include losses of chromosome 19p (55%), 6 (19%) and 19q (13%). Similar to a previous study [14], chromosome 6 loss was associated with the cellular subtype (8/12 vs. 2/28, p < 0.001, chi-square test), but was also more frequent in solid versus cystic HBs (5/10 and 4/34, $p = 0.008$, chi-square test) as well as sporadic versus VHL-associated HBs (7/19 vs. 2/28, $p = 0.01$, chi-square test). There were no other CNVs significantly associated with VHL status, histological subtype or peritumoral cysts.

3.3 | Global DNA methylation patterns

Using DNA methylation-based classification (Heidelberg Brain Tumor Classifier version 11b4) followed by *t*-distributed stochastic neighbor embedding (*t*-SNE) analysis together with a reference cohort of 2801 methylation profiles (comprising 2682 CNS tumors and 119 non-neoplastic samples) [16], all samples could be assigned to the methylation class HB Figure S2,Table S1).

To detect stable methylation subgroups, a subsequent unsupervised consensus clustering of the 47 HBs was performed using the cola framework [19] with different feature selection methods for the top 1000, 2000, 3000, 4000 and 5000 most variable probes, respectively. Various partitioning methods were applied, including hierarchical clustering, *k*-means clustering, spherical *k*-means clustering, partitioning around medoids and model-based clustering. Stability metrics and inspection of the consensus heatmaps clearly revealed most stable partitioning for

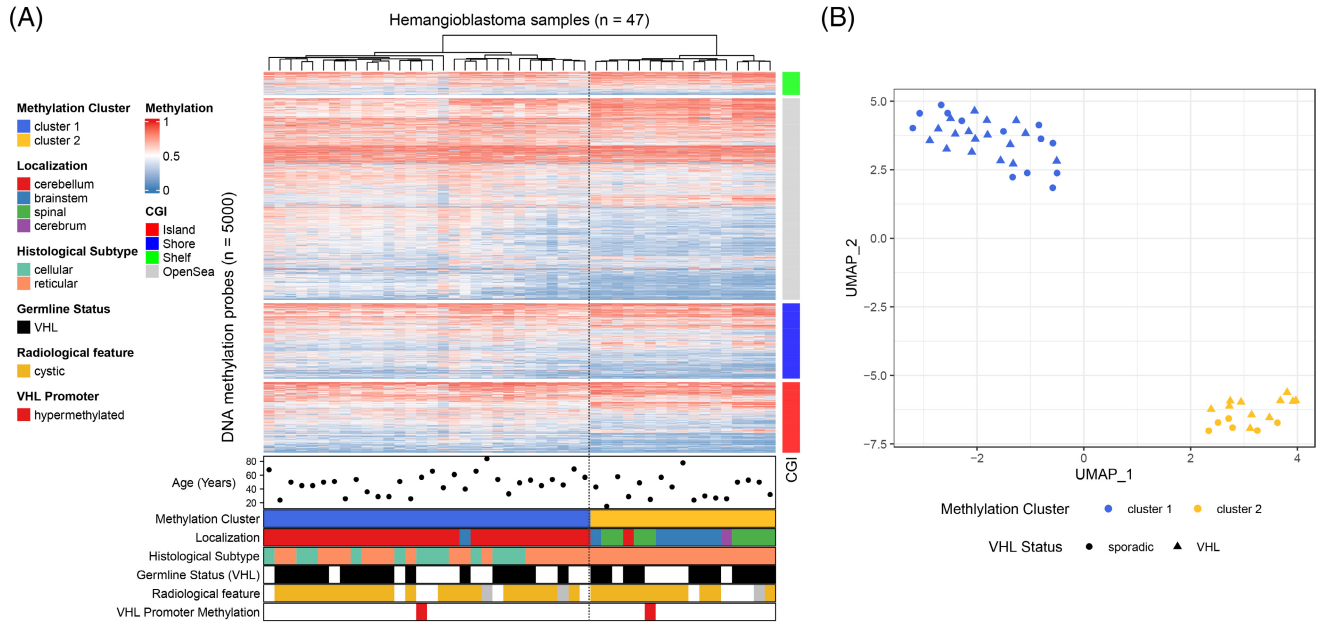

FIGURE 1 Methylation profiling of CNS hemangioblastomas. (A) Unsupervised hierarchical clustering of the 5000 most variable CpG sites (by standard deviation) reveals two clusters. Samples were clustered using the Euclidean distance as the distance measure and Ward's linkage as the clustering method. (B) Unsupervised UMAP analysis confirms the presence of two epigenetic subgroups

2 clusters (Figure 1A, Figure S4). Unsupervised dimensionality reduction using UMAP confirmed the presence of two subgroups (Figure 1B). Consistently, the two clusters also segregate on *t*-SNE analysis (Figure S2). The majority of the 5000 most variable CpGs (2678, 54%) were located in open sea regions that usually overlap with intergenic regions, whereas a rather small fraction (1000 CpGs, 20%) maps to CpG islands which are typically located in gene promoters.

Tumors of methylation cluster 1 comprise 30 HBs (13 sporadic and 17 VHL-associated) of mainly cerebellar location (29/30, Table 1, Figure 1A), whereas methylation cluster 2 contains 17 HBs (6 sporadic and 11 VHL-associated) predominantly arising from noncerebellar locations (8 spinal, 7 brainstem, 1 cerebral and 1 cerebellar) ($p < 0.001$, chi-square test). Of note, 2 of 4 VHL patients with multiple tumors throughout the cohort had HBs of different anatomical locations (HB_13 and HB_30 with each 1 cerebellar and 1 spinal HB) and were assigned to cluster 1 (cerebellar tumors) and cluster 2 (spinal tumors), respectively (Table S1). All 12 cellular HBs were in methylation cluster 1 ($p = 0.003$, chi-square test). VHL germline status and the occurrence of peritumoral cysts were not related to methylation clusters (Table 1). Although the type of copy-number alteration on chromosome 3 (whole chromosomal arm loss or focal 3p25.3 deletion) did not differ between methylation clusters, the overall CNV load (chromosomal regions affected by CNVs in megabases) was significantly higher in cluster 1 versus cluster 2 (262 Mb vs. 109 Mb, $p = 0.001$, Student's *t*-test, Figure 2) with losses of chromosome 6 (affecting 8 cellular and 1 reticular HB) exclusively occurring in this cluster (Table 1, $p = 0.01$, chi-square test). Hypermethylation of the *VHL* promoter was observed in 2 sporadic HBs, one in each methylation cluster (Figure 1A).

3.4 | Differential DNA methylation analysis

We next performed a supervised differential methylation analysis. No significantly differentially methylated CpGs (DMCs) were found when comparing VHL and sporadic as well as cystic and solid HBs, respectively (Figure S5). In contrast, methylation clusters 1 and 2 showed 68,230 DMCs, whereas cellular versus reticular HBs were only slightly different (566 DMCs). Gene Ontology (GO) and KEGG pathway enrichment analysis of DMCs between clusters 1 and 2 revealed several developmental and metabolic terms (Figure S6), but, of note, there were no terms suggestive of neuronal cell contamination in mainly cerebellar cluster 1 tumors.

3.5 | Deconvolution of bulk DNA methylation profiles

Since HBs are composed of neoplastic stromal cells and various non-neoplastic cell types [3], an algorithm for deconvolution of bulk DNA methylomes into latent methylation components was applied [23]. Cross-validation errors and objective values (see methods) pointed towards four distinct methylation components showing stable results across different numbers of input

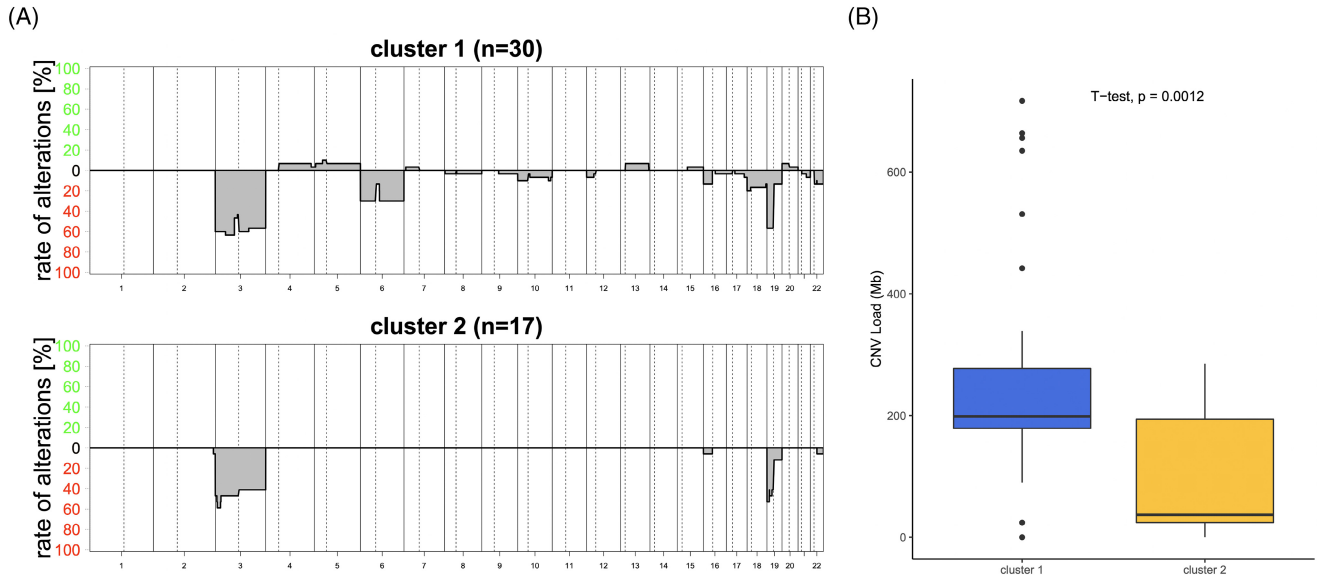

FIGURE 2 Copy-number variations (CNV). (A) Summary CNV plots of methylation cluster 1 (top) and methylation cluster 2 (bottom) show that losses of chr6 among other CNVs exclusively occur in HBs of methylation cluster 1, whereas chr3 and chr 19p losses are equally distributed between both clusters. (B) The CNV load per case, defined as the sum of chromosomal regions affected by CNVs (in Mb), is significantly higher in tumors of methylation cluster 1

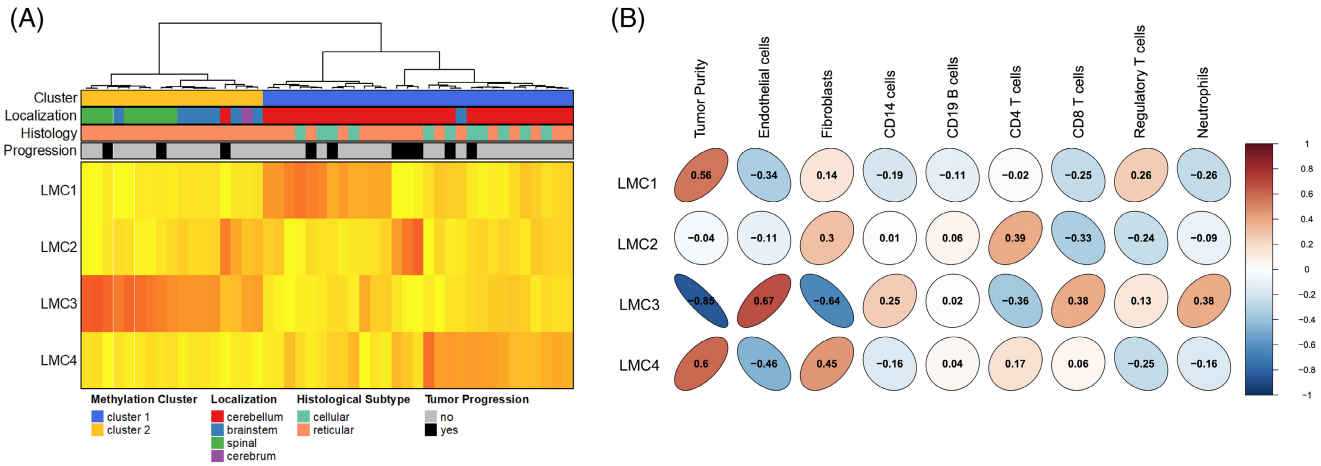

FIGURE 3 Deconvolution analysis. (A) Heatmap showing the proportions of the four latent methylation components (LMC1-4) across tumor samples. Samples were clustered using the Euclidean distance as the distance measure and Ward's linkage as the clustering method. Samples of methylation cluster 1 mainly show high proportions of component 1 or component 4, respectively, whereas component 3 prevails in tumors of methylation cluster 2. (B) Associations between the MethylCIBERSORT proportions and LMC proportions. The Pearson correlations are shown as ellipses that are directed to the upper right for positive and to the lower right for negative correlations, respectively

CpGs for deconvolution analysis (Figure S7). The proportions of these components (LMC1-4) were calculated for each sample and unsupervised hierarchical clustering of the proportions resembled the two global DNA methylation clusters (Figure 3), suggesting that cerebellar and non-cerebellar HBs of methylation clusters 1 and 2 are composed of different methylation components. The 30 tumors of methylation cluster 1 showed significantly higher proportions of components 1 and 4, whereas component 3 was significantly associated with tumors of methylation cluster 2 (Figure 3A, Figure S8). LMC3 and LMC4 were significantly associated with histological subtype (each $p < 0.01$) and LMC1 was associated with the CNV status on Chr3p (chromosomal deletion vs. focal deletion, $p < 0.01$), whereas none of the LMCs was significantly associated with VHL status (Figure S8). We further investigated the four methylation components using the reference-based algorithm MethylCIBERSORT [24] and an estimation of tumor purity [26]. Of note, two different methylation components (components 1 and 4) were positively correlated with tumor purity suggesting that they might represent the main neoplastic cell

components (Figure 3B). Component 3 was characterized by a strong endothelial signature but inverse correlation with tumor purity, and further showed associations with CD8-positive T cells and neutrophils. The strongest association of component 2 was found with CD4-positive T-cells and high proportions of this component were found in individual samples of both methylation clusters 1 and 2. Relevant associations with B cells were not detected.

Furthermore, deconvolution analysis was performed together with other VHL-related tumor entities including 21 endolymphatic sac tumors (ELST, retrieved from GSE168808) and 324 clear cell renal cell carcinomas (ccRCC) of the TCGA cohort (TCGA-KIRC). VHL status was available for all ELST and HB tumor samples. Cross-validation errors and objective values pointed towards 6 LMCs. The proportion heatmap of the resulting 6 LMCs showed a clear separation of HB and ELST from TCGA-KIRC (Figure S9A). Accordingly, LMC1-5 were significantly associated with the tumor type (each $p < 0.05$; Figure S9B). Interestingly, in this large cohort, LMC6 was significantly associated with VHL status in HB and ELST (sporadic vs. VHL, $p < 0.05$, Figure S9B).

3.6 | Patient outcome

Follow-up information could be retrieved for all 42 patients with a median follow-up time of 16 months Table S1). Progressive or new lesions at the same location necessitating neurosurgical intervention were observed in seven patients after a median time of 20 months (range 2–45 months), and mainly affected patients with VHL disease (6/7 patients). We did not observe any growth at the site of previously resected lesions suggesting tumor recurrence after incomplete resection. On Kaplan–Meier analysis, VHL status, histological subtype and methylation cluster showed no significant influence on progression-free survival Figure S10). Similarly, there was no significant influence of LMC proportions to progression-free survival (Figure S11).

4 | DISCUSSION

Using DNA methylation profiling of a large series of sporadic and VHL-associated HBs, two stable molecular clusters were identified. Similar to other CNS tumor entities [17, 27, 28], global methylation patterns were strongly associated with anatomical location and segregate most cerebellar (methylation cluster 1) and non-cerebellar (methylation cluster 2) HBs. As compared to infratentorial IDH-mutated diffuse astrocytomas showing similar methylation profiles in tumors of cerebellar and brainstem origin [28], brainstem HBs clearly segregate from vicinal cerebellar HBs and rather group with spinal HBs (Figure 1). We have therefore also considered non-neoplastic cerebellar tissue contamination as a confounding factor [29] in cluster 1 tumors, but careful tumor tissue dissection as well as GO and KEGG term enrichment analysis argue against this possibility. Furthermore, the methylation clusters differ in their cytogenetic profiles with higher chromosomal instability in cluster 1 tumors, suggesting true biological differences beyond the epigenetic level. Of note, loss of chromosome 6, previously being linked to HB pathogenesis [10, 12], exclusively occurred in cluster 1 tumors, also pointing towards different oncogenic pathways related to methylation clusters. Cellular HBs were exclusively assigned to methylation cluster 1, but this observation was correlated with anatomical location and is in line with previous studies showing a predominance of cellular HBs in the cerebellum [4].

Since tumor DNA methylation profiles are thought to represent a combination of both somatically acquired DNA methylation changes and a signature reflecting the cell of origin [30] that is being maintained throughout tumor progression [31], it is reasonable to assume that cerebellar and non-cerebellar HBs of clusters 1 and 2 might arise from different progenitor cells. Of note, the majority of variable methylation sites between the two clusters overlap with open sea CpG sites which mainly map to intergenic regions that are typically associated with methylation differences among tissues of origin [32]. As part of the CNS brain tumor classifier, HBs have previously been described as a rather uniform subgroup using the Illumina 450 K methylation array platform [16], suggesting that the successor EPIC methylation array mainly harboring additional CpG sites in intergenic regions [33] might help to uncover distinct biological subgroups that are overseen with the 450 K microarray. A previous study has demonstrated transcriptomic dysregulation of genes involved in lipid metabolism such as *ADCY4*, *MGLL*, *ACOT2*, *DGKG*, *SHC1* and *LPAR2* in cystic compared to solid HBs [15], but supervised methylation analysis in our cohort did not identify different methylation in these genes or any other CpGs suggesting that these transcriptional differences are not due to DNA methylation dysregulation. Similarly, there were no global methylation differences in sporadic HBs compared to VHL-related tumors, but, importantly, it needs to be considered that the EPIC methylation array can only detect up to 870,000 CpGs across the entire epigenome containing 28 million CpGs (representing ~3.1% of all CpGs) with improved, but still suboptimal coverage of regulatory elements [33]. Therefore, comprehensive but more costly methods such as whole-genome bisulfite sequencing (WGBS) might help to identify fine-grained differences between clinically different subtypes of HBs.

Beyond differential methylation analysis at individual CpG sites, bulk DNA methylation array data can be used to uncover hidden confounding variation, most importantly different cell type compositions [22, 23]. Given that HBs are histologically composed of neoplastic stromal

cells and non-neoplastic cell types including endothelial cells, pericytes and various immune cells [3], it is reasonable to assume that cluster-specific differences might relate to different cell types. In line with this hypothesis, deconvolution of HB bulk methylation profiles suggested different compositions of cell types, which in turn relate to the two methylation clusters (Figure 3). Furthermore, combining our data with DNA methylation profiles of other VHL-related tumor entities including endolymphatic sac tumors (ELST) and ccRCC revealed a methylation component being associated with VHL status (Figure S9). However, deconvolution methods for DNA methylation array data are still hampered by technical noise and the inability to resolve minor cell types [22]. Therefore, subsequent single cell methods such as single cell RNA sequencing might help to dissect the exact cellular composition of HBs across different biological subtypes.

Taken together, DNA methylation profiling of HBs revealed two distinct epigenetic subgroups that mainly associate with anatomical location (cerebellar vs. non-cerebellar), cytogenetic profiles and differences in latent methylation components. Although global DNA methylation profiles were not associated with clinical outcome parameters, our results indicate that cerebellar and brainstem/spinal HBs have a distinct pathogenesis and might derive from different cells of origin. Examination of a larger cohort including more supratentorial tumors and application of single-cell analysis are warranted.

AUTHOR CONTRIBUTIONS

Conceptualization: Christian Thomas, Markus Holling; Investigation: Niklas Woltering, Anne Albers, Michael Müther, Walter Stummer, Werner Paulus, Markus Holling and Christian Thomas. Analysis and interpretation of the data: Niklas Woltering, Markus Holling, Christian Thomas. Funding acquisition: Markus Holling, Christian Thomas, Michael Müther. All authors were involved in the writing of the manuscript and have read and approved the final version.

ACKNOWLEDGMENT

This project was supported by "Verein von Hippel-Lindau betroffener Familien eV.". CT is supported by DFG (TH 2345/1-1).

CONFLICT OF INTEREST

The authors declare no conflict of interest.

DATA AVAILABILITY STATEMENT

DNA methylation data have been deposited in GEO (accession number GSE197378).

ORCID

Martin Hasselblatt https://orcid.org/0000-0003-2707-8484

Christian Thomas https://orcid.org/0000-0002-6642-7774

REFERENCES

1. Lonser RR, Glenn GM, Walther M, Chew EY, Libutti SK, Linehan WM, et al. von Hippel-Lindau disease. Lancet. 2003; 361(9374):2059–67.
2. Vortmeyer AO, Falke EA, Gläsker S, Li J, Oldfield EH. Nervous system involvement in von Hippel-Lindau disease: pathology and mechanisms. Acta Neuropathol. 2013;125(3):333–50.
3. Vortmeyer AO, Gnarra JR, Emmert-Buck MR, Katz D, Linehan WM, Oldfield EH, et al. von Hippel-Lindau gene deletion detected in the stromal cell component of a cerebellar hemangioblastoma associated with von Hippel-Lindau disease. Hum Pathol. 1997;28(5):540–3.
4. Hasselblatt M, Jeibmann A, Gerss J, Behrens C, Rama B, Wassmann H, et al. Cellular and reticular variants of haemangioblastoma revisited: a clinicopathologic study of 88 cases. Neuropathol Appl Neurobiol. 2005 Dec;31(6):618–22.
5. Louis DN, Perry A, Wesseling P, Brat DJ, Cree IA, Figarella-Branger D, et al. The 2021 WHO classification of tumors of the central nervous system: a summary. Neuro Oncol. 2021;23(8): 1231–51.
6. Pavesi G, Feletti A, Berlucchi S, Opocher G, Martella M, Murgia A, et al. Neurosurgical treatment of von Hippel-Lindau-associated hemangioblastomas: benefits, risks and outcome. J Neurosurg Sci. 2008 Jun;52(2):29–36.
7. Wang Q, Cheng J, Zhang S, Ju Y, Liu W, Hui X. Central nervous system hemangioblastomas in the elderly (over 65 years): clinical characteristics and outcome analysis. Clin Neurol Neurosurg. 2020;189:105622.
8. Liao C-C, Huang Y-H. Clinical features and surgical outcomes of sporadic cerebellar hemangioblastomas. Clin Neurol Neurosurg. 2014 Oct;125:160–5.
9. Oya S, Takayanagi S, Takami H, Indo M, Yamashita T, Saito N, et al. Masked malignant phenotype with a benign appearance: beat-up copy number profile may be the key for hemangioblastoma dissemination. Brain Tumor Pathol. 2021 Jan; 38(1):71–7.
10. Takayanagi S, Mukasa A, Tanaka S, Nomura M, Omata M, Yanagisawa S, et al. Differences in genetic and epigenetic alterations between von Hippel-Lindau disease-related and sporadic hemangioblastomas of the central nervous system. Neuro Oncol. 2017;19(9):1228–36.
11. Muscarella LA, la Torre A, Faienza A, Catapano D, Bisceglia M, D'Angelo V, et al. Molecular dissection of the VHL gene in solitary capillary hemangioblastoma of the central nervous system. J Neuropathol Exp Neurol. 2014;73(1):50–8.
12. Shankar GM, Taylor-Weiner A, Lelic N, Jones RT, Kim JC, Francis JM, et al. Sporadic hemangioblastomas are characterized by cryptic VHL inactivation. Acta Neuropathol Commun. 2014 Dec;24(2):167.
13. Guo X, Gao L, Hong X, Guo D, Di W, Wang X, et al. Whole-exome sequencing and immunohistochemistry findings in von Hippel-Lindau disease. Mol Genet Genomic Med. 2019 Sep;7(9): e880.
14. Rickert CH, Hasselblatt M, Jeibmann A, Paulus W. Cellular and reticular variants of hemangioblastoma differ in their cytogenetic profiles. Hum Pathol. 2006;37(11):1452–7.
15. Wang Q, Liu W, Zhang S, Liang Z, Jiang L, Xue A, et al. Combined transcriptomic and lipidomic analysis reveals aberrant lipid metabolism in central nervous system hemangioblastomas. Sci Rep. 2021;11(1):1314.
16. Capper D, Jones DTW, Sill M, Hovestadt V, Schrimpf D, Sturm D, et al. DNA methylation-based classification of central nervous system tumours. Nature. 2018;555(7697):469–74.

17. Pajtler KW, Witt H, Sill M, Jones DTW, Hovestadt V, Kratochwil F, et al. Molecular classification of ependymal tumors across all CNS compartments, histopathological grades, and age groups. Cancer Cell. 2015;27(5):728–43.
18. Thomas C, Wefers A, Bens S, Nemes K, Agaimy A, Oyen F, et al. Desmoplastic myxoid tumor, SMARCB1-mutant: clinical, histopathological and molecular characterization of a pineal region tumor encountered in adolescents and adults. Acta Neuropathol. 2020 Feb;139(2):277–86.
19. Gu Z, Schlesner M, Hübschmann D. Cola: an R/Bioconductor package for consensus partitioning through a general framework. Nucleic Acids Res. 2021;49(3):e15.
20. Koudijs KKM, Terwisscha van Scheltinga AGT, Böhringer S, Schimmel KJM, Guchelaar H-J. The impact of estimated tumour purity on gene expression-based drug repositioning of clear cell renal cell carcinoma samples. Sci Rep. 2019 Feb 21;9(1):2495.
21. Samuel N, Wilson G, Lemire M, Id Said B, Lou Y, Li W, et al. Genome-wide DNA methylation analysis reveals epigenetic dysregulation of MicroRNA-34A in TP53-associated cancer susceptibility. J Clin Oncol. 2016;34(30):3697–704.
22. Lutsik P, Slawski M, Gasparoni G, Vedeneev N, Hein M, Walter J. MeDeCom: discovery and quantification of latent components of heterogeneous methylomes. Genome Biol. 2017;18(1):55.
23. Scherer M, Nazarov PV, Toth R, Sahay S, Kaoma T, Maurer V, et al. Reference-free deconvolution, visualization and interpretation of complex DNA methylation data using DecompPipeline. MeDeCom and FactorViz. Nat Protoc. 2020;15(10):3240–63.
24. Chakravarthy A, Furness A, Joshi K, Ghorani E, Ford K, Ward MJ, et al. Pan-cancer deconvolution of tumour composition using DNA methylation. Nat Commun. 2018;9(1):3220.
25. Filipski K, Scherer M, Zeiner KN, Bucher A, Kleemann J, Jurmeister P, et al. DNA methylation-based prediction of response to immune checkpoint inhibition in metastatic melanoma. J Immunother Cancer. 2021 Jul;9(7):e002226.
26. Johann PD, Jäger N, Pfister SM, Sill M. RF_Purify: a novel tool for comprehensive analysis of tumor-purity in methylation array data based on random forest regression. BMC Bioinformatics. 2019 Aug;20(1):428.
27. Thomas C, Sill M, Ruland V, Witten A, Hartung S, Kordes U, et al. Methylation profiling of choroid plexus tumors reveals 3 clinically distinct subgroups. Neuro Oncol. 2016 Jun;18(6):790–6.
28. Banan R, Stichel D, Bleck A, Hong B, Lehmann U, Suwala A, et al. Infratentorial IDH-mutant astrocytoma is a distinct subtype. Acta Neuropathol. 2020 Oct;140(4):569–81.
29. Hao X, Luo H, Krawczyk M, Wei W, Wang W, Wang J, Flagg K, Hou J, Zhang H, Yi S, Jafari M, Lin D, Chung C, Caughey BA, Li G, Dhar D, Shi W, Zheng L, Hou R, Zhu J, Zhao L, Fu X, Zhang E, Zhang C, Zhu JK, Karin M, Xu RH, Zhang K DNA methylation markers for diagnosis and prognosis of common cancers. Proc Natl Acad Sci USA. 2017 l 114(28):7414–9.
30. Hovestadt V, Jones DTW, Picelli S, Wang W, Kool M, Northcott PA, et al. Decoding the regulatory landscape of medulloblastoma using DNA methylation sequencing. Nature. 2014;510(7506):537–41.
31. Bormann F, Rodríguez-Paredes M, Lasitschka F, Edelmann D, Musch T, Benner A, et al. Cell-of-origin DNA methylation signatures are maintained during colorectal carcinogenesis. Cell Rep. 2018;23(11):3407–18.
32. Lokk K, Modhukur V, Rajashekar B, Märtens K, Mägi R, Kolde R, et al. DNA methylome profiling of human tissues identifies global and tissue-specific methylation patterns. Genome Biol. 2014;15(4):r54.
33. Pidsley R, Zotenko E, Peters TJ, Lawrence MG, Risbridger GP, Molloy P, et al. Critical evaluation of the Illumina MethylationEPIC BeadChip microarray for whole-genome DNA methylation profiling. Genome Biol. 2016;17(1):208.

SUPPORTING INFORMATION

Additional supporting information may be found in the online version of the article at the publisher's website.

How to cite this article: Woltering N, Albers A, Müther M, Stummer W, Paulus W, Hasselblatt M, et al. DNA methylation profiling of central nervous system hemangioblastomas identifies two distinct subgroups. Brain Pathology. 2022;32(6):e13083. https://doi.org/10.1111/bpa.13083